

# Static Pressure Measurements and Cavitation Signatures on the Nose of a Torque Converter's Stator Blades

Joel Mekkes, Carl Anderson, Amitabh Narain

Department of Mechanical Engineering-Engineering Mechanics  
Michigan Technological University  
Houghton, MI-49931

## EXPERIMENTAL PROCEDURE AND RESULTS

**Test Apparatus.** The experimental stator was designed with fifteen 0.5 mm diameter pressure taps situated in a 3x5 array that wrapped around the nose of the stator. These locations coincided with where the CFD model had predicted a “zero pressure” region to occur. Fig. 5 shows one stator blade and an expanded view of the stator nose showing the location of the pressure taps. The actual stator had only one pressure tap per blade. Each row spanning across the blade from shell to core was given a station number. The station on the pressure side of the blade is called Pressure Station 1 (PS1) and those on the suction side of the blade are called Suction Stations (SS). Pressure taps were located at 0.25, 0.50, and 0.75 of the width of the blade from the shell to the core (S-C). A station number and a shell to core position denote the location of each pressure tap.

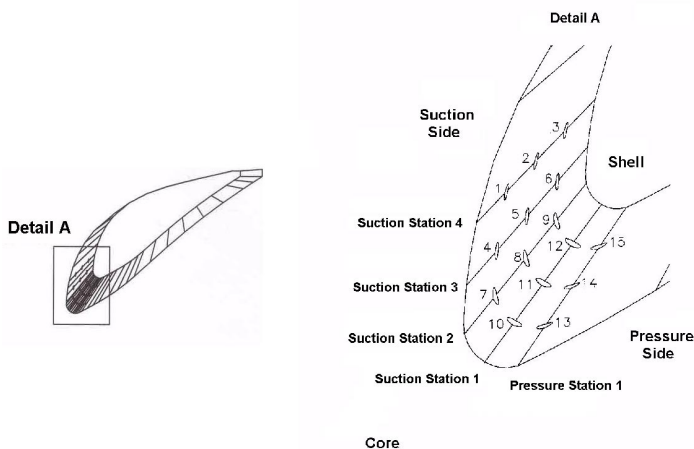


**Figure 4. Location of pressure taps on stator blade.**

The pressure taps were connected to Kulite type XCE-19-093 100 psi absolute pressure transducers located in the hub of the stator through 1 mm manifolds. Each of the pressure manifolds were filled with ATF throughout the pressure tap by letting air escape through an evacuation

hole that was subsequently sealed with a gasket after all the air was evacuated.

The microwave telemetry technique using a single channel transmitter mounted in the stator hub was used to transmit the transducer signals from the stator hub out of the spinning torque converter. Using a time-sequenced multiplexer, a half second of data was transmitted from fourteen of the pressure transducers. The pressure at Pressure Station 6, 0.25 S-C was not sampled, instead a marker channel was used in order to identify which pressure trace belonged to which pressure transducer. The sampling rate for the data was 12800 Hz. Fig. 5 is a photograph of the experimental stator with the cover removed. It shows the telemetry electronics in the hub. Basic details on the microwave telemetry technique can be found in Anderson et al. (2002).



**Figure 5. Stator with cover removed to show telemetry electronics installed in the hub.**

Fig. 6 shows a schematic of the test facility used in this investigation. A 285 HP DC dynamometer was used to drive the pump while the turbine shaft was held stationary by the stall plate. The turbine indexer in the figure was used to change the relative turbine to stator blade position however the results of these investigations are not reported in this paper. A separate hydraulic unit supplied charge pressure to the converter.

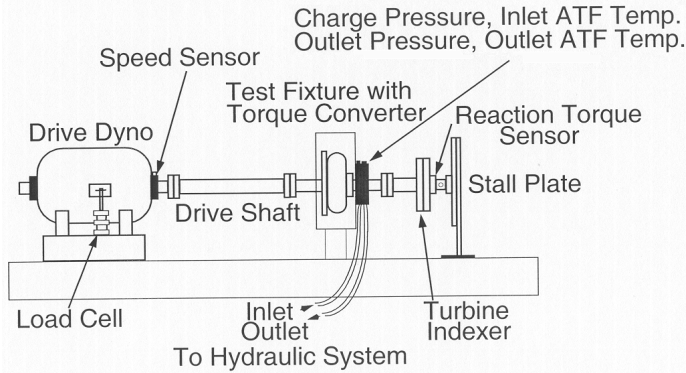
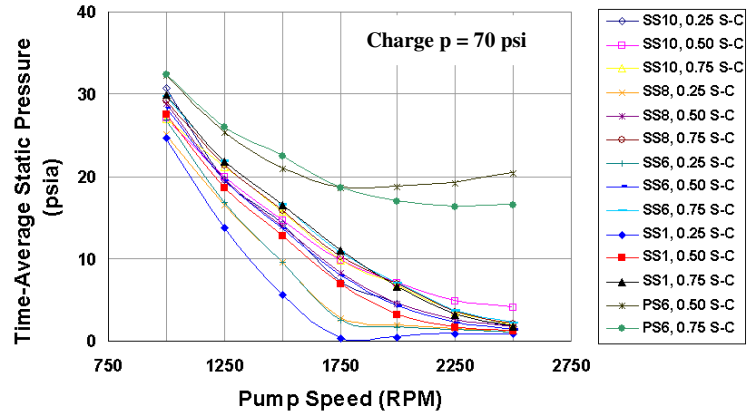


**Figure 6. Schematic of test facility.**

**Test Conditions.** All data were taken at stall condition. Pump speed was varied from 1000 rpm to 2500 rpm in increments of 250 rpm. The charge pressure was varied, in increments of 10 psi, from 70 psi to 130 psi for pump speeds from 1000 rpm to 1500 rpm and 70 psi to 150 psi for pump speeds greater than 1500 rpm. The pressure at the outlet of the converter was kept to a minimum and varied between 4-12 psi during the tested conditions. At all test conditions the inlet temperature was held constant at 80 degrees C and outlet temperature would settle to an equilibrium temperature based on the pump speed and charge pressure. Data was acquired at steady state temperature as long as the outlet temperature was below 120 degrees C. At some of the higher pump speeds, data acquisition was triggered as soon as the exit temperature exceeded 120 degrees C (i.e. before equilibrium was attained). This was to protect the electronics and batteries of the microwave telemetry system from excessive temperatures.

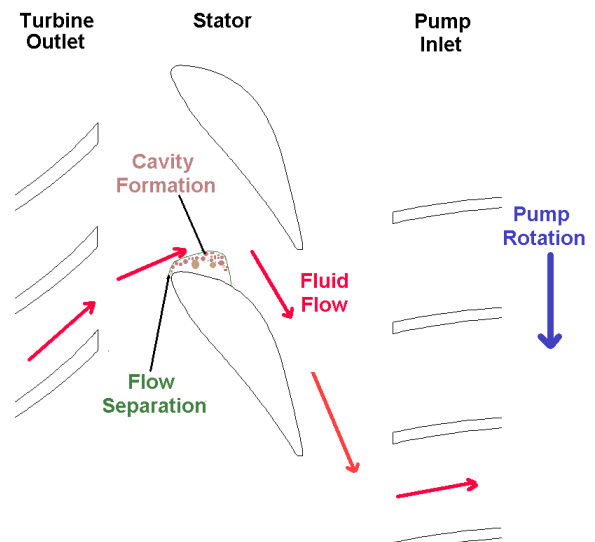
**Results and Discussions.** Fig. 7 shows a time-averaged pressure plot at each pressure tap location as a function of pump speed for a charge pressure of 70 psi. Contrary to the CFD predictions, the static pressure on the pressure side of the blade, PS6, 0.50 S-C and PS6, 0.75 S-C, never dropped to pressures near the saturation pressure of the ATF. At a pump speed of 2500 rpm the time-averaged static pressure over nearly the entire nose of the blade is near the saturation pressure of ATF.

Fig. 7 also shows that the pressure tap located at SS1, 0.25 S-C recorded the lowest time-averaged pressure in the converter. The pressure at this tap was 0.35 psia at a pump speed of 1750 rpm and a charge pressure of 70 psi. The local temperature of the fluid at the stator was not known. However, for the saturation pressure of ATF to be 0.35 psia, the temperature would have to have the unlikely value of being over 160 degrees Celsius.



**Figure 7. Time-averaged static pressure as a function of pump speed at a charge pressure of 70 psi.**

From the measured blade surface static pressure, it is expected (see Mekkes 2003) for the tested operating conditions that an attached cavity does not form on the stator blade nose. Instead, cavitation is thought to be forming in the free-shear layer in the flow separation zone (see Fig. 8). This conclusion is justified by several investigations (Le et al. 1993, Franc and Michel 1985, and Laberteaux and Ceccio 2001) on the formation of cavitation on airfoils at high angles of attack. In all these cases, flow separation occurred and bubble formation was first observed in the shear layer away from the blade. Furthermore surface pressure measurements in a cavitating zone by Le et al. (1993) had a range of values — from nearly vapor pressure during supercavitation to approximately 1.2 psi above the vapor pressure during earlier stages of cavitation. A schematic of the expected formation region of cavitation in the torque converter is shown in Fig. 8.



**Figure 8. Schematic of expected region of cavitation formation.**

A transducer's pressure response,  $p(t)$  is composed of a steady pressure component  $\bar{p}$ , and a fluctuating pressure component,  $p'(t)$ , as

$$p(t) = \bar{p} + p'(t). \quad (1)$$

The fluctuating component of pressure ( $p'$ ) also revealed information about cavitation behavior in the torque converter. At a pump speed of 2000 rpm a representative time trace of pressure, with the mean value set to zero, is shown in Fig. 9 for SS1, 0.25 S-C at two charge pressures: 150 psi and 70 psi respectively. The fluctuating pressure was clearly charge pressure dependent at this constant pump speed.

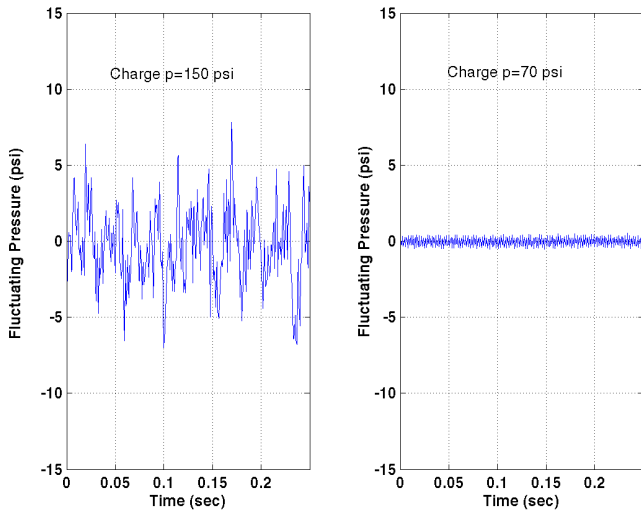


**Figure 9. A representative fluctuating pressure signal  $p'$  at SS1, 0.25 S-C and a pump speed of 2000 rpm with charge pressures of 150 psi and 70 psi.**

The fluctuating pressure  $p'$  in these two plots could be affected by three main reasons: (i) flow fluctuations arising from mechanical forcing functions associated with shaft rotation, various blade passages, etc.; (ii) flow turbulence; and (iii) cavitation. Phenomena (i) and (ii) are not strongly influenced by the value of the charge pressure. In the investigation by Anderson et al. bubble collapse was argued to be the reason for increasing pressure fluctuations with decreasing charge pressure in the pump passage. The observed trend in pressure fluctuations at the nose of the stator blade in this investigation was the complete opposite. It is suspected that cavitation bubbles forming at the nose of the stator blade were attenuating the pressure fluctuations on the blade surface and/or possibly causing a change in the flow structure around

the nose of the stator. Clearly pressure fluctuations increased with increased charge pressure. This was because higher charge pressures delayed/inhibited formation of cavities around the transducers located near to the stator nose.

In the previous investigation by Anderson et al. (2001) the cavitation signature was found to be a broad-band noise. The time domain and frequency domain characterization of fluctuating pressure produced nearly identical results. For this reason, in this investigation, the simpler time domain characterization of the fluctuating pressure ( $p'(t)$ ) was performed using the *mean square pressure MSP*, where

$$MSP \equiv \frac{1}{T} \left( \int_0^T p'^2 dt \right). \quad (2)$$

Fig. 10 shows the mean square pressure of  $p'$  for SS1, 0.25 S-C versus pump speed for each charge pressure tested. At low pump speeds the mean square pressure is nearly the same for all charge pressures. This would indicate cavitation is not occurring in the converter. Even in this zone, as pump speed increases, the mean square pressure increases as would be expected from increased turbulence. However, at or above a pump speed of about 1500 rpm, the fluctuations in pressure become significantly charge pressure dependent. At first the effects of increased turbulence and associated increase in pressure fluctuations dominate the effects associated with increased pump speeds at any given charge pressure. However further increases in pump speeds make the effect of increased formation of cavities - and associated damping of pressure fluctuations at the transducer location - more dominant. Overall, however, lower charge pressures display a lower mean square pressure than the higher charge pressures. As the pump speed is increased the mean square pressure falls nearly to 0 psi<sup>2</sup>. At a pump speed of 2250 rpm all the tested charge pressures have very small fluctuations in the pressure signal.

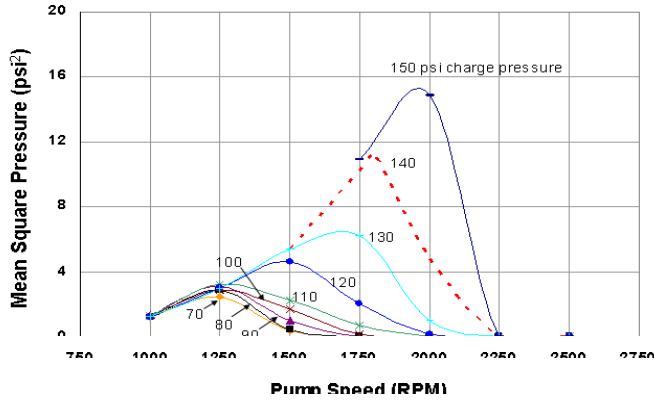


**Figure 10. Mean Square Pressure as a function of pump speed and charge pressure.**

For stall conditions with a steadily rotating pump (at a rotation rate  $\Omega$ ), any time-averaged local flow variable  $\Phi$  (such as MSP) at a point inside a torque converter would depend on quantities that typically determine the solution of the torque converter's boundary value problem. For cavitating flows, one must add charge pressure  $p_c$  (pressure at the inlet to the torque converter) and vapor pressure  $p_v$  (at a representative flow temperature) to the list of parameters that typically determine the flow field in non-cavitating flows. It is easy to see that the variable  $\Phi$  will depend on the shape and size (size is determined by pump diameter  $D$ ) of the torque converter, location of the point in the flow field where  $\Phi$  is measured, pump speed  $\Omega$ , charge pressure  $p_c$ , vapor pressure  $p_v$ , representative mean values of fluid density  $\rho$  and viscosity  $\mu$  at a representative temperature, and inlet-to-exit pressure difference ( $p_c - p_e$ ) which is equivalent to including throughput oil flow rate  $Q$ . As an approximation, it can be assumed that the pressure difference  $p_c - p_e$  is primarily determined by the pump speed  $\Omega$  and only secondarily determined by the throughput flow rate  $Q$ . It can be further assumed that, at reasonably high pump speeds, the Reynolds number  $(\rho D^2 \Omega) / \mu$  is large, so effects of viscosity  $\mu$  are negligible (as is the case for centrifugal pumps under fully rough turbulent flow conditions). Therefore, for a given family of torque converters, a given fluid (ATF), and a given transducer location, the more significant variables affecting  $\Phi$  are given by the assumption:

$$\Phi \cong \text{function}(D, \Omega, \rho, p_c). \quad (3)$$

The dimensionless form of Eqn. 3, for  $\Phi = \sqrt{MSP}$ , is easily obtained (see  $\Pi$ -Theorem in White 1986) and is given by:

$$Ca' \cong \text{function}(\tilde{\Omega}_p), \quad (4)$$

where  $Ca'$  is a nondimensional fluctuating pressure that we refer to as the fluctuating cavitation number and is defined as

$$Ca' \equiv (\sqrt{MSP}) / \left( \frac{1}{2} \rho (D\Omega)^2 \right), \quad (5)$$

and  $\tilde{\Omega}_p$  is dimensionless pump speed defined as

$$\tilde{\Omega}_p \equiv (D\Omega) / (\sqrt{p_c / \rho}). \quad (6)$$

The fluctuating cavitation number at SS1, 0.25 S-C is plotted as a function of dimensionless pump speed in Fig. 11. At dimensionless pump speeds below 1.25 the fluctuating cavitation number displayed a relatively flat behavior. A dimensionless pump speed of 1.25 is the point where a three point running average of the fluctuating cavitation number fell 10% below the steady value. At dimensionless pump speeds greater than 1.25 the fluctuating cavitation number began to drop off sharply. It is thought that at a dimensionless pump speed of 1.25 cavitation bubbles start to form away from the blade and begin to damp the pressure fluctuations near the blade. When a dimensionless pump speed of 1.63 is reached, the fluctuating cavitation number is nearly zero and remains there for all higher values. A dimensionless pump speed of 1.63 was defined as advanced cavitation and is the point where a three point running average was within 10% of the initial value of fluctuating cavitation number at low dimensionless pump speeds. It is thought that advanced cavitation is achieved when the region of bubble formation in Fig. 8 has extended itself all the way to the blade surface. However, a single attached cavity is not expected because the time-averaged static pressures were much higher than the vapor pressure of ATF (see Mekkes 2003).

## function of dimensionless pump speed at SS1, 0.25 S-C

### CONCLUSION

Attenuation of the pressure fluctuations by newly formed and growing gaseous cavities marks the inception of cavitation at the stator blades. The results compared relatively well with the signature of cavitation inception at the downstream locations within the pump passages where enhancement over turbulent pressure fluctuations were observed. This was due to vapor cavities - that were *formed* near stator blade - *collapsed* at locations near the pump passage transducers. This paper demonstrates that the fluctuating component of pressure on the suction side of the stator nose can alternatively be used to detect incipient and advanced cavitation. By this new approach, a dimensionless pump speed of 1.25 and 1.63 marked incipient and advanced cavitation respectively.

The minimum pressure measured did not drop to the saturation pressure of ATF. As a result attached cavitation near the nose of the stator blade was ruled out. The drop in pressure on the pressure side of the blade with increasing pump speed was not in accord with CFD predictions (which, because of turbulence, are only approximate in nature).

### ACKNOWLEDGEMENTS

GM Powertrain, a division of the General Motors Corporation, sponsored this research. The authors wish to express their gratitude to both Don Maddock of GM and Glen Barna of IR Telemetry for technical support.

### REFERENCES

- Anderson, C.L., Zeng, L., Sweger, P. O., Narain, A., Blough, J.R., "Experimental Investigation of Cavitation Signatures in an Automotive Torque Converter using a Microwave Telemetry Technique," 9<sup>th</sup> ISROMAC, February 2002.
- Dong, Y., Dorivi, V., Attibele, P., Yuan, Y., 2002, "Torque Converter CFD Engineering Part II: Performance Improvement through Core Leakage Flow and Cavitation Control," SAE Paper No. 020884.
- Dupont, P., Parkinson, E., Avellan, F., 1993, "Cavitation Development in a Centrifugal Pump: Numerical and Model Tests Predictions," FED, vol. 177, Cavitation Inception- 1993, pp. 63-72.

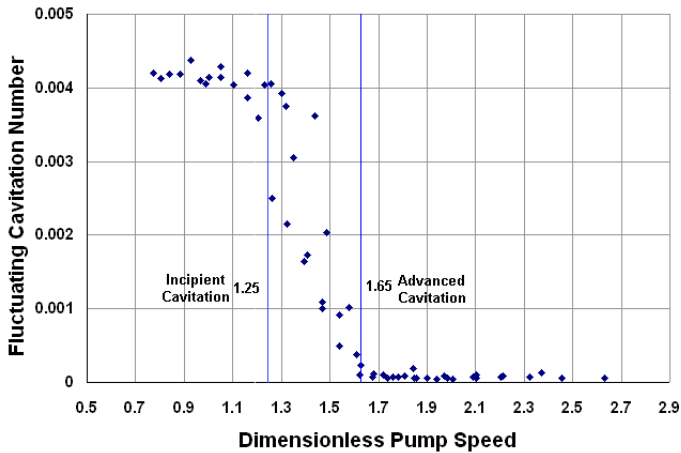


Figure 11. Fluctuating cavitation number as a function of dimensionless pump speed at SS1, 0.25 S-C

The above dimensionless pump speed values compared well with those cited by Anderson et al. (2002) of 1.32 and 1.76 marking incipient and advanced cavitation from fluctuating pressure measurements made in the pump passage for a similar converter.

Fig 12. is a plot of time-averaged static pressure as a function of dimensionless pump speed at SS1, 0.25 S-C. A line at a dimensionless pump speed of 1.63 marking advanced cavitation is shown. The time-averaged pressure reached a value near zero at the dimensionless pump speed marking advanced cavitation. This behavior is probably associated with the coalescence and attachment of the bubble formation zone to the surface where the pressure transducers were mounted.

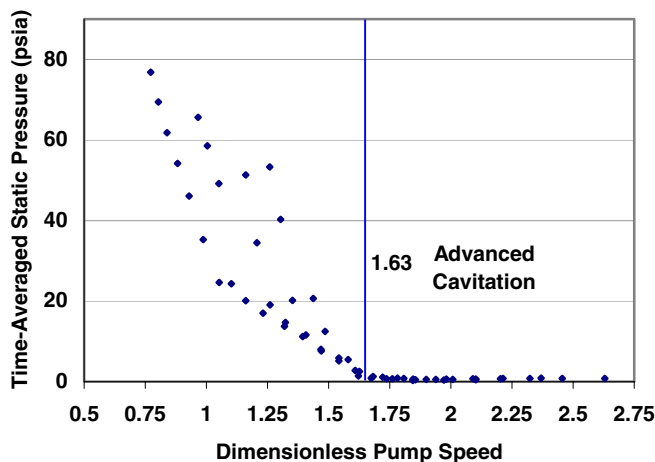


Figure 12. Time-averaged static pressure as a

Ejiri, E., Kubo, M., 1999, "Performance Analysis of Automotive Torque Converter Elements," ASME Journal of Fluids Engineering, vol. 121, pp. 266-275.

Franc, B., Michel, J., 1985, "Attached Cavitation and the Boundary Layer: Experimental Investigation and Numerical Treatment," Journal of Fluid Mechanics, vol. 154, pp. 63-90

Kikuyama, K., Minemura, K., Hasegawa, Y., Murakami, M., 1987, "Unsteadiness of Pressure Distribution and Cavitation Inception on the Impeller Blades of a Centrifugal Pump," JSME (Series B), vol. 493, pp. 2814

Kikuyama, K., Murakami, M., Asakura, E., Hasegawa, Y., 1986, "Effect of Inlet Flow Pattern on Cavitation Inception of Centrifugal Pumps," Bull. JSME, vol. 29, pp. 2522-2528.

Laberteaux, K., Ceccio, S., 2001, "Partial Cavity Flows Part 1. Cavities Forming on Models Without Spanwise Variation," Journal of Fluid Mechanics, vol. 431, pp. 1-41.

Le, Q., Franc, J., Michel, J., 1993, "Partial Cavities: Global Behavior and Mean Pressure Distribution," ASME Journal of Fluids Engineering, vol. 115, pp. 243-247.

Li, S.C., Cavitation of Hydraulic Machinery, Imperial College Press, London, 2000.

Schweitzer, J., Gandham, J., "Computational Fluid Dynamics on Torque Converters – Validation and Application," 9<sup>th</sup> ISROMAC, February 2002.

Watanabe, H., Kurshashi, T., Kojima, M., 1997, "Flow Visualization and Measurement of Torque Converter Stator Blades Using a Laser Sheet Lighting Method and a Laser Doppler Velocimeter," SAE Paper No. 970680.

White, F. M., Fluid Mechanics, McGraw-Hill Inc., 1986.